Catena 194 (2020) 104687

Contents lists available at ScienceDirect

Catena

journal homepage: www.elsevier.com/locate/catena

Properties of carbon particles in archeological and natural Amazon rainforest soils

Sugandha Dogra Pandey[a,*], Leonardo Cristian Rocha[b,c], Gabriel Pereira[c,d], Camila Deschamps[a], João Luiz Elias Campos[a], Newton Falcão[e], André Prous[f], Ado Jorio[a]

[a] Departamento de Física, ICEx, Universidade Federal de Minas Gerais, Av. Antônio Carlos, 6627, 31.270-901 Belo Horizonte, MG, Brazil
[b] Departamento de Geociências, IGC, Universidade Federal de Minas Gerais, Av. Antônio Carlos, 6627, 31.270-901 Belo Horizonte, MG, Brazil
[c] Departamento de Geociências, DEGEO, Universidade Federal de São João del-Rei, Av. Visconde do Rio Preto, S/N, 36301-360 São João del-Rei, MG, Brazil
[d] Programa de Pós-Graduação em Geografia Física, PPGF, Av. Professor Lineu Prestes, 338, 05508-000, São Paulo, SP, Brazil
[e] Coordenação de Tecnologia e Inovação, COTEI, Instituto Nacional de Pesquisas da Amazônia, Av. André Araújo, 2936, Aleixo, 69.060-001 Manaus, AM, Brazil
[f] Setor de Arqueologia Pré-histórica Museu de história Natural e Jardim Botanico da UFMG, Rua Gustavo da Silveira, 1035-Santa Ines, 31.080-010 Belo Horizonte, MG, Brazil

ARTICLE INFO

Keywords:
Terra Preta de Índio
Rio Negro
Carbon
Raman spectroscopy
Scanning electron microscopy
Energy dispersive X-ray spectroscopy

ABSTRACT

Driving practices of Amazon native inhabitants are an example of positive feedback in carbon storage acting as a key element in soil fertility and stability. The anthropogenic Amazonian *Terra Preta do Índio* (Indian Dark Earth) soils are rich in pyrogenic black carbon and the *Rio Negro* (Black River) also exhibits plentiful apparently similar black-carbon particles. In this context, we characterized the structural, morphological and elemental properties of the long-lived stable carbon-based structures present in sediments of the Amazonian *Rio Negro* and in two *Terra Preta do Índio* soils from two different geographic regions. Optical microscopy, Raman spectroscopy, scanning electron microscopy and energy dispersive X-ray spectroscopy techniques are utilized. The structural analysis displayed that these carbon structures exhibit similar nanocrystallite structures, despite their different geographic location and environment. The *Terra Preta do Índio*-carbons are however, more defective and the quantitative elemental analyzes indicate they have greater variety of nutrients, such as P and Ca, than *Rio Negro* sediment-carbons.

1. Introduction

Disordered or amorphous carbon particles are nanocrystalline solid allotropic carbon materials (Kouchi, 2014) and subject of great interest due to a large variety, such as coal, soot, char, carbon black, anthropogenic carbon and other forms of carbon that are neither graphite nor diamond (Dennison et al., 1996). These amorphous carbons are available in nature as a result of human activities (Jorio et al., 2012; Lehmann, 2005; Novotny et al., 2009) and natural phenomena. In this work, we have explored the structural, morphological and elemental differences between anthropogenic and natural carbon, based on their geographical locations and environmental surroundings, to generate a prototype (Jorio et al., 2012) and to understand, among others, how environment and surroundings influences the materials properties. More specifically, micron-sized carbon particles from two different types of samples are analyzed here: (1) anthropogenic soils; and (2) natural river sediments.

The Amazon basin has a variety of soil classes with distinct properties, generally characterized as highly weathered soil, with low fertility and low levels of nutrients and soil organic matter (SOM), such as clayey Ferralsols or sandy Podzols (Glaser and Birk, 2012; Kern et al., 2003; de Souza et al., 2016). However, in midst of these Amazonian land, highly fertile black colored soil exists, known as *Terra Preta do Índio* (TPI) or Amazonian Dark Earths. They are located in a range of soil classes and landscapes with dimensions varying from one hectare to several square kilometers (de Souza et al., 2016). Thus, TPI has been a subject of scientific interest because of their high fertility and long-term stability, and these properties are related to the high amount of carbon-based materials present in the TPI soils (Bezerra, 2015; Cunha et al., 2009; Jorio et al., 2012; Kern et al., 2003; Lehmann, 2005; Pagano et al., 2016; Ribeiro-Soares et al., 2013; Sérgio Ferreira Pessoa Junior et al., 2012). The substances found in *Terra Preta do Índio* soils show that this is the result of human activities (Lehmann, 2005; Ruivo et al., 2003), and the similarities between these soils (Jorio et al., 2012;

* Corresponding author at: Room no. 149, Departamento de Quimica, ICEx, Universidade Federal de Minas Gerais, Av. Antonio Carlos, 6627, 31.270-901 Belo Horizonte, MG, Brazil.
E-mail addresses: sugandha.dogra@gmail.com, adojorio@fisica.ufmg.br (S.D. Pandey).

https://doi.org/10.1016/j.catena.2020.104687
Received 8 October 2019; Received in revised form 24 April 2020; Accepted 16 May 2020

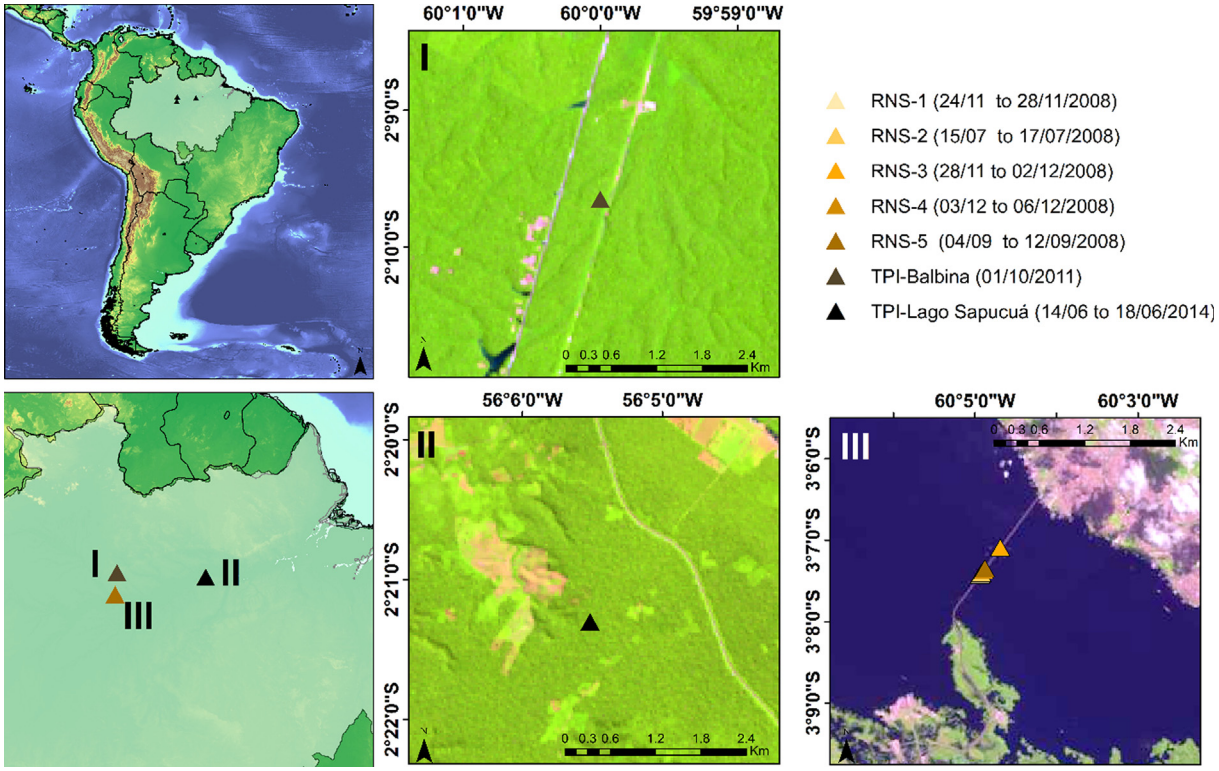

Fig. 1. Dates and locations of collected TPI-soils and RNS samples. (I) TPI sample in Balbina, near Manaus (Amazonas state, Brazil); (II) TPI sample in Lago Sapucuá, in the lower Trombetas River basin, a tributary of the Amazonas river (Pará state, Brazil); and (III) Rio Negro Sediments (RNS) collected in *Rio Negro* bridge, near Manaus City (Amazonas state, Brazil), at depths of 30 to 70 m.

Pagano et al., 2016; Ribeiro-Soares et al., 2013), with similar structural and compositional characteristic of TPI-carbons, despite of location differences (WinklerPrins, 2015) raise the question whether there could be some inspiration behind their formation.

For example, floods from the *Rio Negro* (Black River) could have initiated the early-stage black earth formation that would inspire ancient civilizations. *Rio Negro* is the largest left tributary of the Amazon river and the most famous black water river in the world (Furch, 1984), surrounded by *Terra Preta do Índio* sites (German, 2004). Blackwater rivers derive entirely from soils of lowland forests, rich in leaves and other decaying organic matter. The dark color of the river's water is due to the presence of brown or reddish soluble organic material (humic and fulvic acids) produced by the decomposition of the forest when it is flooded (Horbe et al., 2008) and by the presence of black carbon particles. The presence of black carbon particles signifies that, in the past, primary or secondary forests were burned and generated black carbon residues, which have been brought by rainwater and deposited in the river.

The presence of black carbon materials in both *Terra Preta do Índio* soils and *Rio Negro* sediments thus raises the possibility that floods may have been responsible for triggering a soil amendment with carbon structures, which would be discovered and improved by humans. By itself, the location coincidence cannot be taken as an evidence since the distribution of *Terra Preta do Índio* in the Amazon Region is not limited to black rivers, and the lack of access roads to interior locations make these statements difficult to evaluate (Kern et al., 2003).

To understand differences among various amorphous carbon (Ferrari and Robertson, 2000) forms and how surrounding conditions, environment, and quality of soil influences the properties of the stable carbon particles, we have here carried out an analysis of the structural and compositional aspects of carbon particles present in *Terra Preta do Índio* soils and, *Rio Negro* sediments. Optical microscopy, Raman spectroscopy, scanning electron microscopy and energy dispersive X-ray spectroscopy techniques were used for physical, structural and elemental analysis.

2. Material and methods

2.1. Sample details

For simplicity, from now on we will use the abbreviations TPI and RNS to refer to *Terra Preta do Índio* and *Rio Negro* sediments, respectively.

TPI soils have high level of nutrients (specially of P, Ca and Mn), and organic materials, product of inorganic [e.g. ash, bones (esp. fish)] and organic matter (e.g. biomass wastes, manure, excrement, urine, and biochar), due to alterations of infertile Ferralsols (Fraser et al., 2011; Glaser and Birk, 2012). Most of the known TPI sites found are located near main Amazonians rivers. Although early reports speculate about volcanic ash deposits or sedimentation processes, by now it is accepted that TPI soils are the result of human activity (Lehmann, 2005; Liang et al., 2008; Smith, 1980) created by Amerindian populations before the arrival of Europeans (Lehmann, 2005).

We studied total 58 samples, which includes 5 samples of TPI-Balbina, 5 samples of TPI-*Lago Sapucuá* and 48 samples of RNS. Table S1 (supplementary material) contain detailed information on exact location and depth profile of each sample. The TPI-soils samples were collected in 2011 from Balbina Presidente Figueiredo, Manaus, Amazonas state, Brazil (Pagano et al., 2016), and in 2014 from the bank of *Lago Sapucuá*, in the lower Trombetas River basin, a tributary of the Amazonas river, Pará state, Brazil, approximately 500 km far from the previously studied TPI samples (Ribeiro-Soares et al., 2013). We have studied TPI-soil samples from different locations of Amazonas state to corroborate the similarities between carbon structure of TPIs, despite of distances.

RNS were collected in 2008 from Ponte do *Rio Negro*, Manaus, Amazonas state, Brazil, which included sediments from depths of 30 – 70 m (Technosonda), as shown in Fig. 1.

Fig S1 (supplementary material) shows the depth profile of RNS. The RNS were collected at various depths to observe the difference in with time and effect of nature and environment on carbon structure. We have also observed that,as the depth increases, the amount of carbon particle reduces, and the color of sediments becomes lighter. The lower percentage of carbon in deeper region can be explained considering the deeper sediments have been deposited longer, and the more superficial sediments are more recent. If we consider the time factor, the deeper particles are being weathered for longer periods, so there will be a lower carbon contents.

2.2. The Amazon basin (Auxiliary data)

In this study, auxiliary data were used to explain the dynamical process regarding the TPI sample analyses. The Tropical and Subtropical Wetlands Distribution version 2 from the Center for International Forestry Research (CIFOR) was used to indicate the carbon storage in peatlands areas (Verchot et al., 2017). This product covers the subtropics and tropical regions of the globe with wetland and peak information to the geographical region between 180°W to 180°E and 40°N to 60°S, excluding small islands, with a spatial resolution of 231 m, derived from satellite soil moisture estimation, geomorphological data, and a hydrological model to indicate the water flow and areas of wetness. The aboveground biomass density of vegetation was acquired from (Avitabile et al., 2016), representing a merge from several datasets with a spatial resolution of 1 km. Also, the geological information was derived from the Brazilian Institute of Geography and Statistics (IBGE) with the lithologic classification of the geology of the Amazon Basin (available at www.ibge.gov.br).

Furthermore, the Fire products MOD14 and MYD14 of Moderate Resolution Imaging Spectroradiometer (MODIS) sensor were used to estimate the fire density in the study area is shown in fig. S2 (supplementary material). The MOD14 and MYD14 are daily products with 1 km spatial resolution at nadir with almost 4 acquisitions per day (01:30 am, 10:30 am, 13:30 pm and 10:30 pm). To estimate fire density, a convolution mask $\omega(\gamma,\kappa)$ with C × L (columns × lines) overpasses the fires location ϑ(longitude and latitude), resulting in a 4-km Gridded image data (Fire-Grid) with accumulated fires to the study area for the period of 2002–2018, where the convolution mask overpasses the entire image (longitude $\in [\alpha, C-\alpha]$, latitude $\in [\beta, L-\beta]$), as described in Eq. (1).

$$Fire\_Grid_{(lon,lat,t)} = \sum_{\gamma=-\alpha}^{\alpha} \sum_{\kappa=-\beta}^{\beta} \omega(\gamma, \kappa)\vartheta(lon + \gamma, lat + \kappa, t) \quad (1)$$

2.3. Characterization methods

2.3.1. Optical microscopy analysis

The physical appearance of TPI soil and RNS was perceived by Nikon eclipse-DS-Fi2 optical microscope with a 20× objective. The microscopy images were captured using NIS-element F 4.00.00 software. Each sample was prepared by taking approximate 5 mg of sample dissolved in 5 ml of deionized water (DI), with a slighter volume dropped on the separate glass coverslip and analyzed after drying at room temperature.

2.3.2. Electron microscopy analysis

For the topography and the qualitative elemental composition of the carbon grains of TPI soil and RNS, SEM and EDXS techniques were used. SEM micrographs of randomly collected carbon grains of TPI soil and RNS were measured. Among the grains chosen manually, some have distinct physical characteristics inherent to black carbon. Twenty five SEM images and twenty sevenEDXS analysis indicated that there are differences in the composition of each black grain chosen. SEM images were carried out by a Dual Beam electron microscope. An Esprit Bruker Nano GmbH equipment was used for EDXS analysis with a primary energy of 15kev. The EDXS is an elemental analysis technique based on the generation of characteristic X-rays that reveals the presence of elements in the samples. The peak position in the EDXS spectrum on energy axis, classifies the specific element. The element identification and their percentage are generally achieved using manufacturer's software (Scimeca et al., 2018). The EDXS spectrum contains both semi-qualitative and semi-quantitative information and it is used in the study of environment pollution, detection of heavy metals pollution and in medical and biological fields (Scimeca et al., 2018). In addition, SEM with EDX was shown as an effective way of determining elemental composition, such as C and O present in biochar (Ma et al., 2016). Moreover, surface morphology and mineral elements (Na, K, Ca, Mg, P) present in biochar were analyzed by using SEM/ EDX (Liang et al., 2016; Suárez-Hernández et al., 2017). For SEM/EDX analysis we placed around 1 mg of soil sample on a glass slide and then picked black grains under a microscope. Randomly collected dark grains of each specimen were placed on a sample holder.

2.3.3. Raman spectroscopy analysis

Confocal Raman Spectroscopy was used to confirm the presence of carbon in RNS and TPI soils and to determine their structure (Ferrari and Robertson, 2000; Jorio et al., 2012; Pagano et al., 2016; Ribeiro-Soares et al., 2013). Raman spectra were acquired with Andor™ Technology-shamrock sr-303i spectrometer coupled with a charge-coupled device (CCD) detector, in the backscattering configuration, using 60X oil immersion objective lens of a Nikon inverted microscope. Excitation was provided by 488 nm (2.54 eV) laser with the exposure time 60 s on each sample. A Neon lamp was used to calibrate the spectra for spectral range of (505–643 nm). Whenever the experiment was performed, each time the spectrometer was calibrated to maintain accuracy.

2.3.3.1. Sampling procedure. Raman experiments were carried out on randomly selected black grains of carbon found in TPI soil and RNS of various depths. Approximately 2 mg of RNS and TPI soil samples were separately dissolved in 5 ml of DI water, and a slighter volume dropped on the separate glass coverslip and measured after drying at room temperature. The Raman signal from the carbon structures is suppressed by the presence of sand and other elements present in the soil. Therefore, it is essential to place a small amount of sample on coverslip, and to locate carbon particle for observing a strong Raman signal. On the contrary, carbon particle would be covered or combined with dust/sand, generating large background overcoming the Raman signal.

2.3.3.2. Spectral fitting. Total of 244 Raman spectra of arbitrarily selected black carbon particles of TPI soils and RNS were acquired. For statistical analysis, background correction is needed to access Raman spectroscopic information. The Protocol given by (Ribeiro-Soares et al., 2013) was employed to all spectra for linear baseline correction between 800 cm^{-1} and 1900 cm^{-1} by using the PeakFit software. The major spectroscopic signature was given by the G (1584 cm^{-1}) and D (1350 cm^{-1}) bands. The G band is a result of in-plane stretching of the sp^2 carbon bonds, whereas the D band is due to vibration activated by the presence of structural defects in a non-perfect sp^2 hexagonal structure.

2.3.3.3. Parameterized Principal component analysis. Principal Component Analysis (PCA) (Jolliffe, 2002) is a technique for dimensionality reduction and feature extraction that consists of calculating the directions of significant variance in a data set. PCA performs coordinate transformation where each new axis represents a direction of data variation, and ordering these axes in descending order of importance, so the first component (axis) represents the most significant variance in the data, and so on. To make PCA useful for automated classification of sp^2 carbon structures, (Campos et al., 2017) presented the concept of parametrization that enhanced some selected

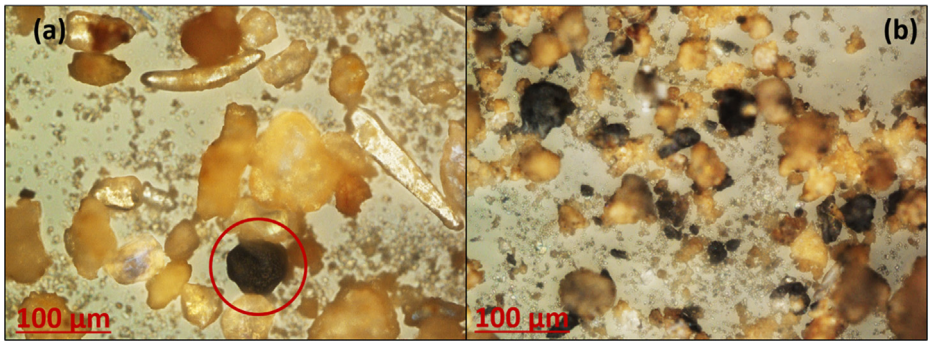

Fig. 2. Optical microscopy image of (a) RNS and (b) TPI soil. The red circle highlights a black carbon grain in RNS.

features, obtained from reference samples, and use these features for structural sample classification.

3. Results and discussion

3.1. Physical characteristics

Table S1 (supplementary material) describes the physical appearance as observed (via optical microscope) and the lithology of all 58 samples of RNS and TPI soils. For RNS samples, lithology description was provided by the company-Technosonda, who made the drilling. Fig. 2 represents the optical microscope image of RNS and TPI soil samples showing the presence of black carbon particles. The optical analysis shows that RNS samples have much fewer quantities of black grains than TPI samples. The distributions of black carbon in TPI samples are more homogeneous and all samples are dark in color and moist in appearance and the grains are neither as thin nor as thick as those found in the soils of the RNS. Both samples have fish bones, and several fish bones are larger in RNS. Presence of fish bones and organic amendments (biomass wastes, manure and, biochar) in TPI soils were also perceived by (Glaser and Birk, 2012). Visually, the texture of the RNS is varying according to the depth at which the samples were collected. The variations are found in color and elements present in the soil and, as the depth increases, the presence of black particles decreases. The samples closer to the surface are grayish brown, similar to the mud, and the grain sizes are generally smaller than 0.05 mm, also containing small pieces of dried leaves, fragments of fish bones, and many black carbon grains. In the deep region samples, the color becomes yellow and begin to resemble sand, the grains sizes are approximately between 0.05 and 2 mm, and the samples have a few fragments of fish bones, and rare black carbon grains were found.

3.2. SEM and EDXS

SEM micrographs of carbon grains of TPI soil have porous morphology and RNS have sandy morphology, although some RNS samples are also accompained by porous carbons, specially carbons found between 35 and 45 m of depth, see Fig. 3. The porous carbon found in RNS might be the result of forest burning. Qualitative elemental composition using EDX (Figs. 4a and 4b) showed that the higher percentage of carbon was found in samples with porous characteristics, not sandy. Here it is important to stress that EDX provides semi-qualitative and semi-quantitative information limited to a tiny amount of material, thus bringing issues with respect to the homogeneity of samples, but we generalize the discussion here based on several arguments. TPI-soil have a large number of black particles (Fig. 2) but the percentage of carbon in them is less than the porous carbon found in RNS, and this could be due to the fact that TPI-soil has long term exposure to the environment. The porous carbon found in RNS has more percentage of carbon because it is not exposed to the external environment, unlike TPI soil. Thus, the general trend of EDX analysis showed that the percentage of carbon in RNS-carbon reduces as depth increases, and TPI-carbon has a greater variety of nutrients, such as phosphorus and calcium in its composition than RNS. Considently, the TPI-Balbina soil composition reported by Pagano et al. (2016) showed a higher presence of organic matter and nutrients (P, Ca, Mn, and K). Glaser and Birk (2012) also reported high nutrients (P, Ca and Mn) and Organic matter in TPI soil. The higher percentage of these nutrients in TPI soil are because of successive incorporation of organic products by Ameridians. In contrast, these elements will be more scarce in the RNS because they are natural sediments that suffering over geological weathering, thus bases are leached. Thus, weathering and local geology directly interfere with these chemical elements or nutrients. The TPI soil also exhibits a higher concentration of Al than the RNS. The presence of Fe is significant in RNS. In general, black water has more iron than white water (Horbe et al., 2008). The presence of silicon, potassium, titanium, gold and palladium is also more frequent in RNS. The elemental composition is depth-dependent for TPI-soil, while TPI-carbon structure was independent of depth (Pagano et al., 2016). The quantitative elemental analysis of TPI-carbon and RNS-carbon presented that the elemental composition of carbon depends on surrounding/location and depth.

Fig. 4a indicates that the natural carbon in the RNS is high, except RNS-2 and RNS-5. The relatively smaller percentage of carbon in these two samples could be due to these reasons:

(I) The RNS-2 sample from the survey data is characterized as medium to coarse brown sand, very compacted. Such characteristics are restricted to the carbon accumulation, due to the colloidal characteristics of the sandy sediments and the lower porosity.
(II) The RNS-5 (45.23 m) sample is characterized by being a red and hard clay structure with no organic matter, and there are no conditions for carbon accumulation due to sediment compaction and lack of organic matter shortage.

The percentages of the RNS-2 and RNS-5 are relatively lower when compared to the other natural carbon rates of the river (Fig. 5a), but with values very close to the anthropic carbon of the TPI-Lago Sapucuá (Fig. 4b). The samples RNS-1,3,4 and 5 (42.5 m) have organic clays in their composition, being the explanation for the relatively high values of natural carbon (Fig. 5b). The reason for the expressive values for the natural carbon in the *Rio Negro* is the Peatlands as can be seen in Fig. 5c. When observing the Peatlands, several high densities in the drainage heads are found. The same pattern is observed in areas near the samples collected in the *Rio Negro* bridge. Another relevant factor that must be considered is the accumulation of sediments over thousands of years, since the collections in the fluvial channel are in an average depth of 44 m. Animal bones (fish) are also observed in sediments, as can be seen in Fig. 2.

The explanation for the higher concentration of carbon in Balbina is the moisture content, because it is close to the encounter of drainage (Fig. 5c). Therefore, the anthropic carbon of Balbina is potentiated by environmental issues. Another factor that could explain the Balbina

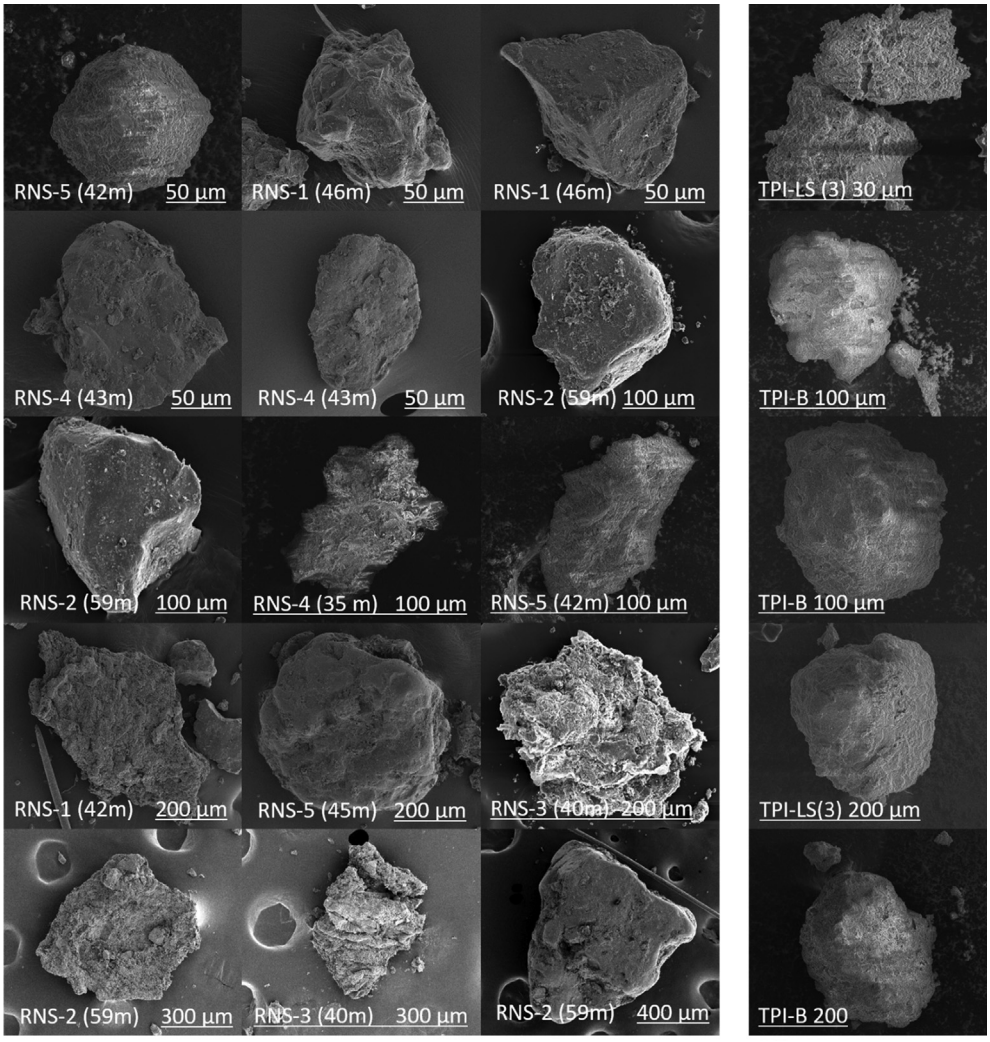

Fig. 3. Scanning electron microscopy topography of carbon grains observed in RNS (5X3 images on the left side) and TPI soil (5X1 images on the right side).

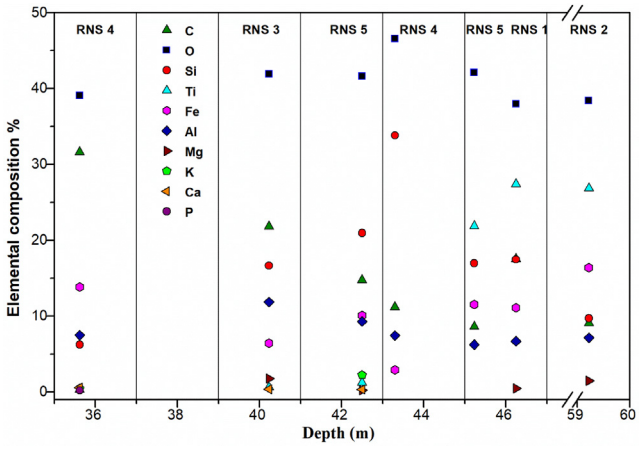

Fig. 4a. Percentage of elements present in Sediments of Rio Negro (RNS 1 to 5). The information comes from EDXS and, as such, it represents a semi-quantitative trend.

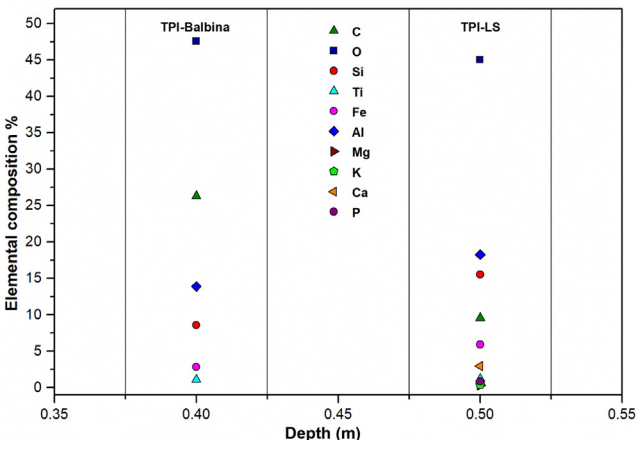

Fig. 4b. Percentage of elements present in TPI-Balbina and TPI-*Lago Sapucuá*. The information comes from EDXS and, as such, it represents a semi-quantitative trend.

samples characteristics is the geology. The geological patterns indicate that sandstone and clays of the formation Alter do Chão leads to formation of clayey soils that, by the colloidal properties, accumulate organic matter. The geology of *Lago Sapucuá* is formed by concretions of irons, being materials resulting from high intemperance processes that do not favor the accumulation of organic matter.

The physical characteristics of TPI soil (Balbina and *Lago Sapucuá*) are very similar, regardless of geographic location. The soil particles are heterogeneous, rounded of varying sizes, quite porous. But in spite of the physical similarity from the images, there are enough differences

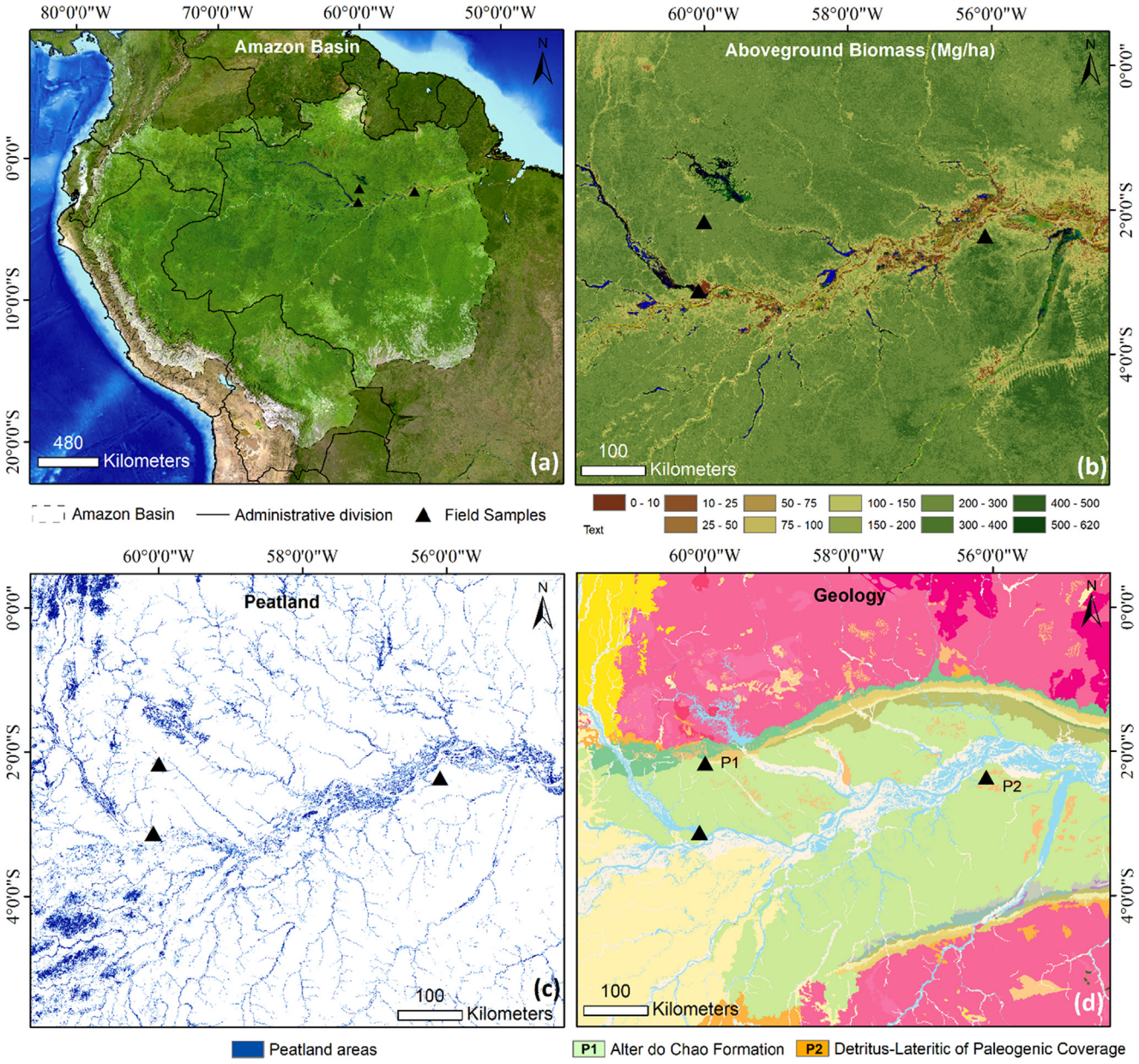

Fig. 5. (a) Amazon basin with the TPI-soils samples (Black triangles); (b) Aboveground biomass (in Mg/ha) and TPI-soils samples; (c) Derived peatland areas and TPI-soils samples; and (d) Lithologic classification of the geology of the Amazon Basin and TPI-soils samples over Alter do Chao formation (TPI sample in Balbina, near Manaus, Amazonas state, Brazil) and Detitus-Lateritic of Paleogenic Coverage (TPI sample in Lago Sapucuá (LS), in the lower Trombetas River basin, a tributary of the Amazonas river, Pará State, Brazil).

from the geochemical point of view. The silica data had also many differences. The silica from TPI-*Lago Sapucuá* is almost double of the TPI-Balbina, and this percentage can be explained by the geological location. The higher percentage of Fe, Al, and Bauxite in the *Lago Sapucuá* are related to geological properties, which are characterized by lateritic debris cover. The percentages of oxygen are very similar, as well as the titanium data. In relation to Mg, P, K and Ca, these elements are null in TPI-Balbina, but are found in very low percentages in the TPI-*Lago Sapucuá*.

Another dynamic process that affects the analysis of samples is fire occurrence (Fig. S2). Fires are an important tool to land use and land cover changes in Amazon, converting the Amazon Rainforest into grassland and agricultural areas. Thus, fires could be associated with several effects in erosion, runoff, soil properties, water management and in the ecosystem components (Neary et al., 2005). The fire radiative power released during biomass burning modify the physical, chemical, and biological properties of the soil due to transformations in chemical components caused by fire temperature and in water retention caused by vegetation ashes. Consequently, nitrogenous compounds and vaporized organic matter are transferred to deeper and cooler soil layers, changing the soil structure (Debano et al., 1976; Parro et al., 2019).

Soil organic matter (SOM) is associated with the biological decomposition and concentrates in the first layer of the soil. At high temperatures, SOM is converted into pyrogenic organic compounds resulting in changes in aggregate stability, pH and minerals composition (Santín and Doerr, 2016). An example of changes in SOM properties is the anthropogenic soils, such as TPI, which the addition of ash/charcoal and other material (fish bones and waste) to Amazon poor nutrient soils, produced a fertile soil when compared with adjacent soils (Glaser and Birk, 2012; McMichael et al., 2014).

Furthermore, when addressing the RNS, it is observed that the

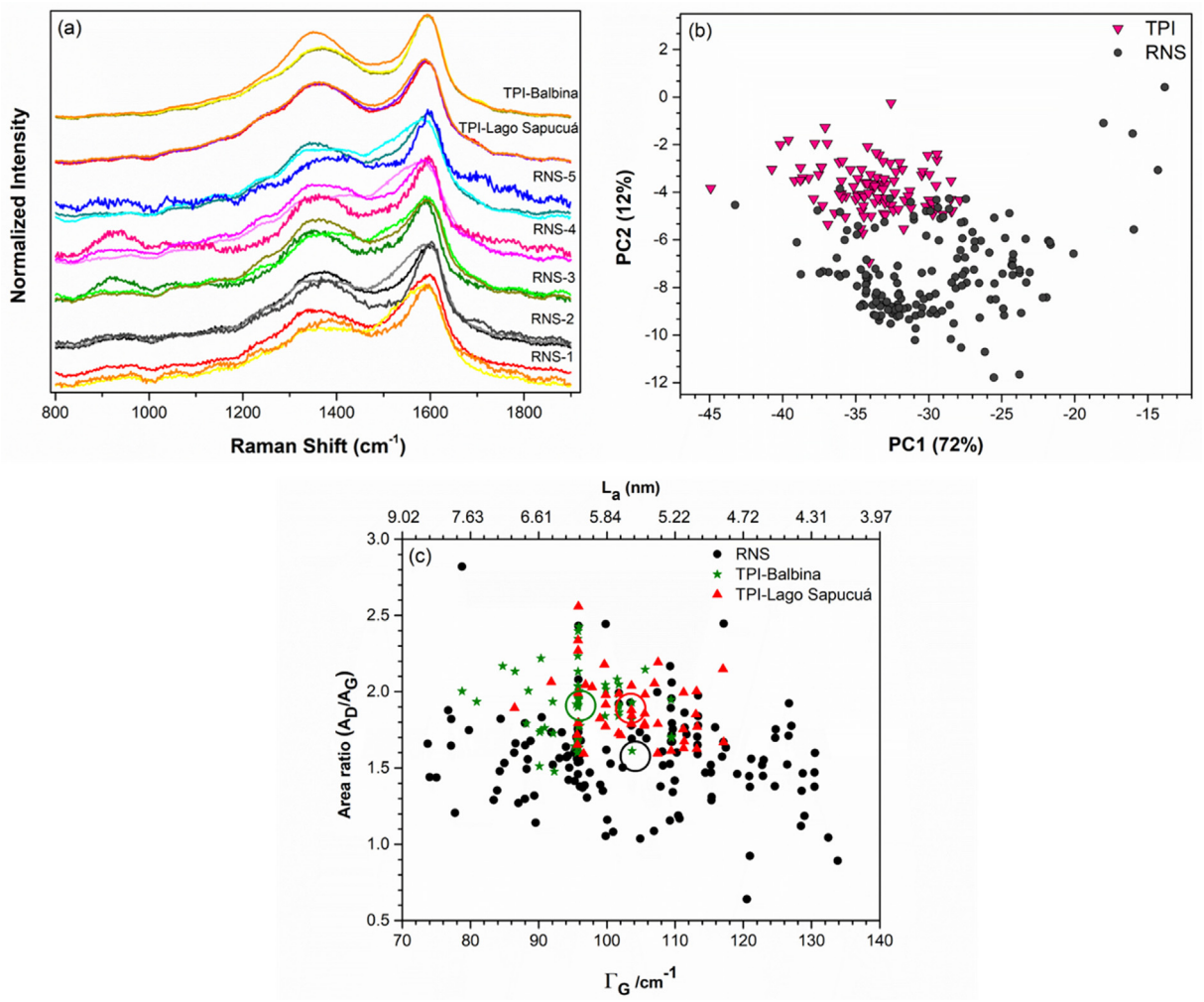

Fig. 6. (a) Raman spectra of RNS (1–5) and TPI-carbon from Balbina and Lago Sapucuá (LS), (b) Parametrized PCA showing PC1 × PC2 plot of TPI and RNS, (c) The Area ratio of G and D bands (A_D/A_G) vs full-width at half maximum of G band (Γ_G) for RNSs and TPIs of Balbina and Lago Sapucuá (LS) (see legends). The highlighted empty circle shows the average values for the data. The top x-axis shows the crystallite size of observed carbon grains, calculated according to Ref. (Ribeiro-Soares et al., 2013).

sediments are small, rounded, thin and some elongated. It must be taken into account that these sediments are in an average depth of 44 m, therefore the weight caused by deposition may be able to deform the sediment. These samples present very similar geochemical properties; the only exception is the RNS-4 (43.3 m) which presents high silicon content.

3.3. Raman spectroscopy

For structural analysis, we acquired 244 Raman spectra, out of which 58 were from TPI-Balbina, 44 from TPI-*Lago Sapucuá* and 142 from RNS carbon. Fig. 6 (a) shows Raman spectra of black carbon grains of RNS and TPI soils after baseline subtraction, between 800 cm^{-1} to 1900 cm^{-1}. The major spectroscopic signature was given by the G (1584 cm^{-1}) and D (1350 cm^{-1}) bands. The spectra obtained from TPI soil are mostly the same, although a few spectra of TPI-Balbina are different in terms of intensity and full width at half maximum (FWHM). Most of the obtained spectra of TPI soil show good agreement with the previously studied TPI samples (Jorio et al., 2012; Pagano et al., 2016; Ribeiro-Soares et al., 2013). Raman spectra of TPI-carbon was obtained with high-intensity counts, showing nature of well-stabilized carbon bond, which might be an indication of carbon present in TPI soil has a long time of exposure to environment, acquiring a most stabilized structure. At the same time, TPI spectra are accompanied by a more amorphous character in comparison to RNS-carbon. Some of the carbon structure of RNS also have structural similarity with nanographitic carbon because the wavenumber of G band reaches to 1580 cm^{-1} downwards. The observed Raman signal of RNSs and TPI soils majorly comes from sp^2-hybridized carbon-like structure, although we cannot rule out the presence sp^3 hybridization, as a visible light excites mostly sp^2 π electron bands (Jorio et al., 2012). Structural analysis of these sp^2-hybridized carbon using parametrized PCA displayed higher point defect in TPI-carbon in comparison to RNS-carbon (Campos et al., 2017), evidenced in Fig. 6 (b) by the higher average values of PC2 weights. For details, see (Campos et al., 2017). This is consistent considering TPI soil is formed by a highly reactive carbon material, ideal for soil enrichment.

For a better understanding of the PCA result, Raman spectra were fitted with two Lorentzian peaks for the G and D band. Wavenumbers (ω_G, ω_D), FWHMs (Γ_G, Γ_D), and the integrated intensity (area) ratio (A_D/A_G) range values are tabulated in Table S 2 (supplementary material). Variation of Γ_G and A_D/A_G ratio depend upon the structure of carbon (Cançado et al., 2017; Ferrari and Robertson, 2000; Jorio et al., 2012; Pagano et al., 2016; Ribeiro-Soares et al., 2013). Fig. 6 (c) shows the plot of the integrated intensity (area) ratio A_D/A_G and Γ_G. The Γ_G of RNS deposits are varying between 73 cm^{-1} and 135 cm^{-1}, and Γ_G of TPI samples are between 79 cm^{-1} and 117 cm^{-1}, which is attributed to crystallite size. We have plotted the secondary axis which shows the

crystallite size distribution with respect to Γ_G, calculated using (Ribeiro-Soares et al., 2013), showing that as the FWHM increases the crystallite size decreases. On average, Γ_G (L_a) is similarly spread for RNS and TPI soil. With the help of the empty circle, we have shown the average values. Differences in the A_D/A_G ratio distribution are significant when comparing the data from RNS and TPI soil, the TPI samples being higher than the values for the RNS, indicating more defects present in the TPI-carbon structure (Cançado et al., 2017). As we can see from the area ratio and FWHM graph (Fig. 6c), the majority of RNS-carbon has a lower area ratio than the TPI-carbon. Furthermore, there is overlapping in the area ratio graph, as mentioned in SEM Section 3.2. TPI carbon has porous morphology, and RNS-carbon has both sandy and porous morphology and those porous RNS-carbon could possibly be the result of forest burning. Thus, we see a structural similarity between TPI soil and RNS carbon.

4. Conclusion

Optical characterization, Raman spectroscopy, and electron microscopy were applied to characterize the black carbon material found in samples of RNS and TPI soils from two different regions. This study helped us to understand how the surrounding conditions, environment and soiĺs quality influences the structure and properties of carbon. The optical analysis shows that RNS have much fewer quantities of black grains than TPI samples. SEM of TPI-carbon have porous morphology and RNS-carbon have sandy morphology. RNS also exhibit some porous carbon especially between 35 and 45 m of depth. The porous carbon found in RNS might be the result of forest burning.

The EDXS results indicated that the percentage of carbon in RNS-carbon reduces as depth increases, and TPI-carbon has a greater variety of nutrients, such as phosphorus and calcium in its composition than RNS. The TPI-Balbina soil composition reported by Pagano et al. (2016) showed a higher presence of organic matter and nutrients (P, Ca, Mn, and K). Glaser and Birk (2012) also reported high nutrients (P, Ca and Mn) and Organic matter in TPI soil. Thus we observed the similarities with elemental composition of previous studied TPI sites. The physical characteristics of TPI soil (Balbina and *Lago Sapucuá*) are very similar, regardless of geographic location, the soil particles are heterogeneous, rounded of varying sizes, quite porous. But in spite of the physical similarity analyzed by the images, there are enough differences from the geochemical point of view. Mg, P, K and Ca are found in TPI- *Lago Sapucuá,* and we did not observe them in TPI-Balbina.

Finally, we stress that Raman spectroscopy has been established as one of the most powerful techniques for addressing the molecular structure of sp^2-sp^3 carbon materials, due to the sensitivity of the electron-phonon interaction (Campos et al., 2017; Cançado et al., 2017; Ferrari and Robertson, 2000). It applies for general materials science and (Jorio et al., 2012; Pagano et al., 2016; Ribeiro-Soares et al., 2013) for specific applications to the Terra Preta do Índio problem. Our Raman spectral analysis, both spectral fitting and parametrized PCA, suggested that the black carbon structures are similar with respect to sp^2 carbon nanocrystallite size distribution, while the TPI-carbon samples exhibit a more defective structure. This information is consistent with SEM and EDXS qualitative analysis, which showed that the TPI-carbon have a greater variety of nutrient elements. This information cannot be used to conclusively state there is a relation between the two materials, but they can assertively be used to conclude that, from the black-carbon structure, which is the most important piece on the stability of the Terra Preta do Indio soil, the assumption that floods may be at the route of the learning procedure from ancient civilizations that started producing the Terra Preta do Índio soil cannot be ruled out.

Declaration of Competing Interest

The authors declare that they have no known competing financial interests or personal relationships that could have appeared to influence the work reported in this paper.

Acknowledgements

AJ acknowledges Profs. Dorothy Hosler and Heather Lechtman for prompting out the main question addressed in this work. SDP acknowledge CNPq (Project Number- 401135/2014-4, Process Number-314731/2014-8) fellowship. The authors acknowledge CPRM and the Technosonda company who provided the samples.

Appendix A. Supplementary material

Supplementary data to this article can be found online at https://doi.org/10.1016/j.catena.2020.104687.

References

Avitabile, V., Herold, M., Heuvelink, G.B.M., Lewis, S.L., Phillips, O.L., Asner, G.P., Armston, J., Ashton, P.S., Banin, L., Bayol, N., Berry, N.J., Boeckx, P., de Jong, B.H.J., Devries, B., Girardin, C.A.J., Kearsley, E., Lindsell, J.A., Lopez-Gonzalez, G., Lucas, R., Malhi, Y., Morel, A., Mitchard, E.T.A., Nagy, L., Qie, L., Quinones, M.J., Ryan, C.M., Ferry, S.J.W., Sunderland, T., Laurin, G.V., Gatti, R.C., Valentini, R., Verbeeck, H., Wijaya, A., Willcock, S., 2016. An integrated pan-tropical biomass map using multiple reference datasets. Glob. Chang. Biol. 22, 1406–1420. https://doi.org/10.1111/gcb.13139.

Bezerra, J., 2015. In: Terra Preta de Índio and Amazonian History BT - The Brazilian Amazon: Politics, Science and International Relations in the History of the Forest. Springer International Publishing, Cham, pp. 15–58. https://doi.org/10.1007/978-3-319-23030-6_2.

Campos, J.L.E., Miranda, H., Rabelo, C., Sandoz-Rosado, E., Pandey, S., Riikonen, J., Cano-Marquez, A.G., Jorio, A., 2017. Applications of Raman spectroscopy in graphene-related materials and the development of parameterized PCA for large-scale data analysis. J. Raman Spectrosc. https://doi.org/10.1002/jrs.5225.

Cançado, L.G., Campos, L.E., Gomes, M., Martins-ferreira, E.H., Achete, C.A., Capaz, R.B., Jorio, A., 2017. Disentangling contributions of point and line defects in the Raman spectra of graphene-related materials. 2D. Mater. 4, 25039. https://doi.org/10.1088/2053-1583/aa5e77.

Cunha, T.J.F., Madari, B.E., Canellas, L.P., Ribeiro, L.P., Benites, V. de M., Santos, G. de A., 2009. Soil organic matter and fertility of anthropogenic dark earths (Terra Preta de Índio) in the Brazilian Amazon basin. Rev. Bras. Ciência do Solo. doi: 10.1590/S0100-06832009000100009.

Debano, L.F., Savage, S.M., Hamilton, D.A., 1976. DIVISION S-7 — FOREST AND RANGE SOILS. The Transfer of Heat and Hydrophobic Substances During Burning. SOIL SCI. SOC. AM. J. 40, 3–6.

Dennison, J.R., Holtz, M., Swain, G., 1996. Raman spectroscopy of carbon materials. Spectroscopy 11, 38–45.

Ferrari, A.C., Robertson, J., 2000. Interpretation of Raman spectra of disordered and amorphous carbon. Phys. Rev. B 61, 14095–14107. https://doi.org/10.1103/PhysRevB.61.14095.

Fraser, J., Teixeira, W., Falcão, N., Woods, W., Lehmann, J., Junqueira, A.B., 2011. Anthropogenic soils in the Central Amazon: from categories to a continuum. Area 43, 264–273. https://doi.org/10.1111/j.1475-4762.2011.00999.x.

Furch, K., 1984. Water chemistry of the Amazon basin: The distribution of chemical elements among freshwaters. In: Sioli, H. (Ed.), The Amazon: Limnology and Landscape Ecology of a Mighty Tropical River and Its Basin. Springer, Netherlands, Dordrecht, pp. 167–199. https://doi.org/10.1007/978-94-009-6542-3_6.

German, L.A., 2004. Ecological praxis and blackwater ecosystems: A case study from the Brazilian Amazon. Hum. Ecol. 32, 653–683. https://doi.org/10.1007/s10745-004-6831-1.

Glaser, B., Birk, J.J., 2012. State of the scientific knowledge on properties and genesis of Anthropogenic Dark Earths in Central Amazonia (terra preta de Ìndio). Geochim. Cosmochim. Acta 82, 39–51. https://doi.org/10.1016/j.gca.2010.11.029.

Horbe, A.M.C., Oliveira, L.G. de S., 2008. Química de igarapés de água preta do nordeste do Amazonas - Brasil. Acta Amaz. doi: 10.1590/S0044-59672008000400020.

Jolliffe, I.T. (Ed.), 2002. Introduction BT - Principal Component Analysis. Springer New York, New York, NY, pp. 1–9. doi: 10.1007/0-387-22440-8_1.

Jorio, A., Ribeiro-Soares, J., Cançado, L.G., Falcão, N.P.S., Dos Santos, H.F., Baptista, D.L., Martins Ferreira, E.H., Archanjo, B.S., Achete, C.A., 2012. Microscopy and spectroscopy analysis of carbon nanostructures in highly fertile Amazonian anthrosoils. Soil Tillage Res. 122, 61–66. https://doi.org/10.1016/j.still.2012.02.009.

Kern, Dirse Clara, D'aquino, G., Rodrigues, T.E., Frazao, F.J.L., Sombroek, W., Myers, T. P., Neves, E.G., 2003. Distribution of Amazonian Dark Earths in the Brazilian Amazon BT - Amazonian Dark Earths: Origin Properties Management. In: Lehmann, J., Kern, Dirse C, Glaser, B., Wodos, W.I. (Eds.), Springer Netherlands, Dordrecht, pp. 51–75. doi: 10.1007/1-4020-2597-1_4.

Kouchi, A., 2014. Amorphous Carbon BT - Encyclopedia of Astrobiology. In: Amils, R., Gargaud, M., Cernicharo Quintanilla, J., Cleaves, H.J., Irvine, W.M., Pinti, D., Viso, M. (Eds.), Springer Berlin Heidelberg, Berlin, Heidelberg, pp. 1–2. doi: 10.1007/978-3-642-27833-4_70-2.

Lehmann, J., 2005. Terra Preta de Indio. In: Encyclopedia of Soil Science, Second Edition. CRC Press, pp. 1–4. doi: 10.1081/E-ESS-120045010.
Liang, B., Lehmann, J., Solomon, D., Sohi, S., Thies, J.E., Skjemstad, J.O., Luizão, F.J., Engelhard, M.H., Neves, E.G., Wirick, S., 2008. Stability of biomass-derived black carbon in soils. Geochim. Cosmochim. Acta 72, 6069–6078. https://doi.org/10.1016/j.gca.2008.09.028.
Liang, H., Chen, L., Liu, G., Zheng, H., 2016. Surface morphology properties of biochars produced from different feedstocks 1205–1208. doi: 10.2991/iccte-16.2016.210.
Ma, X., Zhou, B., Budai, A., Jeng, A., Hao, X., Wei, D., Zhang, Y., Rasse, D., 2016. Study of biochar properties by scanning electron microscope – energy dispersive X-ray spectroscopy (SEM-EDX). Commun. Soil Sci. Plant Anal. 47, 593–601. https://doi.org/10.1080/00103624.2016.1146742.
McMichael, C.H., Palace, M.W., Bush, M.B., Braswell, B., Hagen, S., Neves, E.G., Silman, M.R., Tamanaha, E.K., Czarnecki, C., 2014. Predicting pre-Columbian anthropogenic soils in Amazonia. Proc. R. Soc. B Biol. Sci. 281, 20132475. https://doi.org/10.1098/rspb.2013.2475.
Neary, D.G., Ryan, K.C., DeBano, Leonard F., 2005. Wildland Fire in Ecosystems: Effects of Fire on Soil and Water. Herpetol. Rev. 4, 250. https://doi.org/10.1021/ac102195x.
Novotny, E.H., Hayes, M.H.B., Madari, B.E., Bonagamba, T.J., deAzevedo, E.R., de Souza, A.A., Song, G., Nogueira, C.M., Mangrich, A.S., 2009. Lessons from the Terra Preta de Índios of the Amazon Region for the utilisation of charcoal for soil amendment. J. Braz. Chem. Soc. 20, 1003–1010. https://doi.org/10.1590/S0103-50532009000600002.
Pagano, M.C., Ribeiro-Soares, J., Cançado, L.G., Falcão, N.P.S., Gonçalves, V.N., Rosa, L.H., Takahashi, J.A., Achete, C.A., Jorio, A., 2016. Depth dependence of black carbon structure, elemental and microbiological composition in anthropic Amazonian dark soil. Soil Tillage Res. 155, 298–307. https://doi.org/10.1016/j.still.2015.09.001.
Parro, K., Köster, K., Jõgiste, K., Seglinš, K., Sims, A., Stanturf, J.A., Metslaid, M., 2019. Impact of post-fire management on soil respiration, carbon and nitrogen content in a managed hemiboreal forest. J. Environ. Manage. 233, 371–377. https://doi.org/10.1016/j.jenvman.2018.12.050.
Ribeiro-Soares, J., Cançado, L.G., Falcão, N.P.S., Martins Ferreira, E.H., Achete, C.A., Jorio, A., 2013. The use of Raman spectroscopy to characterize the carbon materials found in Amazonian anthrosoils. J. Raman Spectrosc. 44, 283–289. https://doi.org/10.1002/jrs.4191.
Ruivo, M.L., Glaser, B., J, S.I., Kern, D.C., Glaser, B., Amazonian, W.I.W., Springer, M., 2003. Amazonian Dark Earths. doi: 10.1007/1-4020-2597-1.
Santín, C., Doerr, S.H., 2016. Fire effects on soils: The human dimension. Philos. Trans. Roy. Soc. B Biol. Sci. 371, 28–34. https://doi.org/10.1098/rstb.2015.0171.
Scimeca, M., Bischetti, S., Lamsira, H.K., Bonfiglio, R., Bonanno, E., 2018. Energy dispersive X-ray (EDX) microanalysis: A powerful tool in biomedical research and diagnosis. Eur. J. Histochem. 62, 89–99. https://doi.org/10.4081/ejh.2018.2841.
Sérgio Ferreira Pessoa Junior, E., Broni de Souza, W.B., dos Santos de Souza, K., Pereira Santana, G., Célio da Silveira Pio, M., 2012. Terra preta de indio na região amazónica. Sci. Amaz. 1, n. 1, 1–8.
Smith, N.J.H., 1980. Anthrosols and human carrying capacity in amazonia. Ann. Assoc. Am. Geogr. 70, 553–566.
de Souza, L.C., de Lima, H.V., Rogrigues, S., Kern, D.C., da Silva, Ã.P., Piccinin, J.L., 2016. Chemical and physical properties of an anthropogenic dark earth soil from Bragança, Para, Eastern Amazon. Acta Amaz. 46, 337–344. https://doi.org/10.1590/1809-4392201505663.
Suárez-Hernández, L.N., Ardila-A.A., Barrera-zapata, R., 2017. Morphological and physicochemical characterization of biochar produced by gasification of selected forestry species Caracterización morfológica y fisico-química de biocarbones producidos. 26, 123–130.
Verchot, L., Wittmann, F., Murdiyarso, D., Roman-Cuesta, R.M., Gumbricht, T., Herold, M., Herold, N., Householder, E., 2017. An expert system model for mapping tropical wetlands and peatlands reveals South America as the largest contributor. Glob. Chang. Biol. 23, 3581–3599. https://doi.org/10.1111/gcb.13689.
WinklerPrins, A.M.G.A., 2015. Terra Preta The Mysterious Soils of the Amazon Antoinette. 287, 235–246.